Moiré Superlattices of Zn^{2+} Mediated 2D Assembly of Mn^{2+}-Cysteine Complex Nanoparticles Alter Electron Spin Transitions in the X-band

Archismita Hajra[a], *Arun Chattopadhyay** [a,b]

[a]Centre for Nanotechnology, Indian Institute of Technology Guwahati, Guwahati, 781039, India

[b]Department of Chemistry, Indian Institute of Technology Guwahati, Guwahati, 781039, India

Corresponding Author

*Arun Chattopadhyay

Orcid id. https://orcid.org/0000-0001-5095-6463

Email id: arun@iitg.ac.in

Keywords: Moiré • 2D film • complex nanoparticle • Electron Spin Resonance • Mn^{2+} ion

Abstract.

Ambient reaction-mediated assembly of cysteine-based nanoparticles of Mn complex, and Zn^{2+} ion led to the generation of moiré patterns in 2D films. Individually formed crystalline 2D films made of manganese cysteine complex nanoparticles and Zn^{2+} ions were stacked angularly against each other giving rise to the moiré films. Selected area electron diffraction patterns revealed a wide range of twist angles. Circular dichroism peaks appearing at 480 nm, 513 nm, and 643 nm; representing moiré chirality were observed irrespective of the chiral identity of the constituent ligand. The moiré films were constituted of two chemically different types of Mn^{2+} ions as revealed by electron spin resonance (ESR) spectroscopy. The ESR signal of Mn^{2+} ion was found to have been altered upon formation of the moiré films as a result of the prevalent interfacial magnetic field of the individual 2D films. The current work focuses on the generation of self-assembled moiré materials of manganese cysteine nanoparticles by Zn^{2+} ion and the influence of so formed moiré pattern on the chemical environment of the Mn^{2+} ions. The discovery of inorganic complex nanoparticle-based moiré material can offer structural, physical, and chemical diversity to materials science.

Introduction

Molecular materials can be defined as functional materials comprised of individual molecules connected through molecular bonds. The molecular bonds help adapt the materials under diverse chemical environments. In addition to covalency,[1] the expansive domain of molecule-based materials chemistry is governed by π-π interaction,[2] dipole-dipole interaction,[3] London force,[4] donor-acceptor coordination interaction,[5] van der Waals force,[6] and metal-metal bonding.[7] The implementation of molecular chemistry in the field of materials science can outgrow the potential of classical inorganic, and organic chemistry. Two-dimensional self-assembly of cobalt-based coordination complex molecule as single-molecule magnet,[8] aggregation of derivatives of phenanthrocarbazole as dual-light emitting species,[1] switching between optical, magnetic, and electrical properties in spiro-molecular materials,[9] spin cross-over phenomenon observed in organic nanoporous metal-organic framework at room temperature,[10] heat-resistant photoluminescence observed in 2D platelets self-assembled in solid/solution phase;[11] dimension dependent magnetic[12] and optical properties[13] of inorganic complex nanomaterials; these are significant attributes of manifestation of molecular chemistry in materials science. The versatility offered by molecular chemistry in materials science is yet to be fully realized. Considering that, the extension of

coordination chemistry, organic chemistry, and inorganic chemistry to materials science can be regarded deemed important.

The evolution of 2D materials since the invention of graphene[14] has enriched materials chemistry in the aspect of understanding the influence of lattice-dimensionality in the achievement of new physical and chemical properties. Following graphene, phosphorene, and boron-based 2D materials, atomically thin transition metal dichalcogenides are also important, and their physical properties owing to their distinctive band-gap varying from system to system have been studied.[15] A few physical phenomena resulting from crystalline 2D assembly may include Raman scattering enhancement, strain effects, optical properties of 2D materials, application of 2D materials in memory devices, quantum hall effect, and heterostructure catalysis.[16,17] The synthetic procedure for these 2D materials has been limited to physical methods, such as mechanical exfoliation, sputtering, chemical vapor deposition, and molecular beam epitaxy for a long time.[16] Lately, reaction-mediated solution state chemistry paved a new way for the synthesis of 2D materials by complexation reaction-mediated assembly of atomic clusters.[18] The lattice dimensionality, and structural rigidity offered by the 2D assembly of atomic clusters have been found to significantly influence the optical, and chemical properties of the pristine clusters.[19,20] This complexation-reaction-mediated assembly of atomic clusters to form 2D materials widened the scope for molecule-based 2D materials. Recently, hybrid 2D structures made of atomically thin metal layers and organic ligands;[21] and coordination complexes[8] have been reported. Previously, molecule-based nanoparticles were obtained,[12,13] now imitating the 2D assembly of atomic clusters by complexation reaction, the idea of a 2D assembly of molecular nanoparticles by similar complexation reaction was also imaginable.

Twisted stacking of 2D films by the means of physical force, such as van der Waals led to generate a new form of material, moiré solid.[22] This introduced a new degree of freedom for tuning the structure of 2D materials - the twist angle.[23] Controlling the number of 2D sheets stacked against each other,[24] and the twist angle[23] between them, a plethora of mechanical, physical, and chemical properties could be attained. For heterostructure 2D materials, lattice-mismatch[25] has also been reported to be an important parameter to generate moiré patterns. The unique structural phenomenon depending on the twist-angle, and lattice-mismatch has been reported to result in alteration in the band structure[25] of the materials, for example, twisted bilayer graphene with a twist angle $\leq 10^{o}$ gave rise to moiré Bloch band.[26] Tuneable flat bands has been considered a distinctive feature of the materials.[27] Moiré

superstructures have been reported to exhibit versatile physical phenomena, such as atypical superconductivity,[28] Mott insulation,[29] orbital magnetism,[30] Chern insulation,[31] quantum Hall states,[32] entropy-activated electronic phase transition.[33] The chemical-bond-driven moiré structures obtained by stacking of 2D crystalline assembly of molecular nanoparticles can come up with another set of possibilities by allowing us to manipulate the chemical bonds involved therein.

In addition to the expanding potential for physical, and chemical properties of moiré solid at the macroscopic level, the possibility of novel quantum-mechanical phenomena arising out of the structure might be of interest. The layered materials emerging as a fertile field for quantum technology owing to their ability to host optically active qubits has secured its recognition in the applications of quantum communication, quantum computations, and quantum sensing.[34] On the other hand, molecular conductors having an intensely correlated electron system, have been reported to present a wide platform for studying quantum mechanical properties, such as quantum spin liquid ground state, the coupling between charge and magnetic degrees of freedom, Mott insulation, and ferroelectricity.[35,36]

Herein, we report the formation of moiré solid by angular stacking of 2D films made of Mn^{2+}-cysteine (Mn-Cys) complex nanoparticles through further complexation reaction by Zn^{2+} ions. The formation of the moiré structure introduced ligand-independent chirality to the system as a consequence of rotational distortion between the crystalline layers. The chemical environment of the constituent metal ion (Mn^{2+}) was probed with electron spin resonance (ESR) spectroscopy and was found to be profoundly altered by the formation of the moiré structure. The alteration in the local chemical environment was reflected in the hyperfine splitting pattern of ESR, as well as in g-values. Presumably, the moiré structure induced an additional field opposing the ligand field to the system, which led the zero-field splitting term of Kramer ion Mn^{2+} to have been heavily perturbed.

RESULT AND DISCUSSION

Complexation by Zn^{2+} ion: Moiré film formation

The uniform-sized (<4 nm) Mn-Cys inorganic complex nanoparticles were prepared as dispersion after completion of a minimum of 24 h reaction followed by centrifugation of the large particles.[37] The dispersion containing poorly crystalline Mn-Cys nanoparticles were subjected to assemble by complexation reaction with Zn^{2+} ions. The reaction was allowed to continue for at least 24 h, till the mixture turned opaque in this course of time. The visual

change in the reaction mixture indicated a possible chemical change. Hence, transmission electron microscopy (TEM) images (Figure 1) were acquired for the sample to obtain morphological details about the newly formed species.

TEM images (Figure 1A-B) revealed the occurrence of a definite kind of pattern resembling lattice fringes appearing in high resolution, which are typically known as moiré patterns.[25] They roughly appeared to be misaligned stacking of two or more crystalline 2D sheets of widely dispersed nanoparticle film (Figure 1A-B). The selected area electron diffraction (SAED) pattern obtained from this region (Figure 1C) was neither a single crystalline nor polycrystalline pattern. The diffraction pattern appeared to be comprised of both single crystalline, and polycrystalline components.

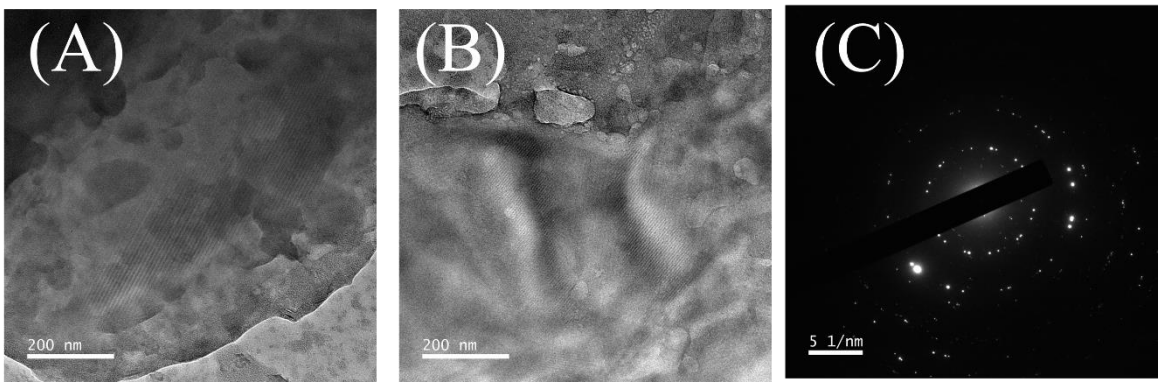

Figure 1. (A-B) Transmission electron microscopy images of the 2D films with ~~of~~ the moiré pattern and (C) SAED pattern recorded from the area.

It could be a result of misaligned stacking of ordered arrangements of amorphous (poorly crystalline) nanoparticles, and crystalline 2D sheets formed on the surface of the nanoparticles. Here the moiré pattern was not just the angularly rotated stacking of well-defined separated 2D films, consisting of hexagonal assembly of surface manganese ions, and zinc ions, and nearly crystalline arrangement of the nanoparticles underneath. The probable lattice parameter (d) values of the constituent nanocrystals were obtained from experimentally observed twist angle, and moiré parameters using Eqn. (1), and correlated with experimentally observed lattice-parameters. The equation can be written as

$$D = \frac{d}{Sin(\frac{\varphi}{2})} \quad \text{.....Eqn (1)}$$

For example, moiré periodicity of 2.63 nm, 5.2 nm, and 12 nm could be correlated with a twist-angle of 3° for experimentally obtained lattice parameters obtained from the SAED patterns of the 2D moiré films (0.069 nm, 0.136 nm, and 0.314 nm). Thus spacing between moiré fringes (D), and the angle of twisting (φ) could be correlated in terms of lattice parameters (d) of the constituent crystals.

The addition of Zn^{2+} ions to the dispersion of widely separated nanoparticles could result in several possibilities. One, reaction-mediated 3D crystalline assembly formations of the dispersed nanoparticles could occur, two, complexation of Zn^{2+} with the remaining precursor in the reaction medium might occur to give 2D sheets made of a new complex that involves Mn^{2+}, Zn^{2+}, cysteine, and acetate ion; three, and lastly, there could be a possibility of complexation on the surface of the nanoparticles available. The experimental observations preclude the formation of the larger assembled nanoparticles. On the other hand, the presence of a low concentration of the ligands after 24 h of initial addition and nanoparticle formations may not have led to film formations. Finally, the third scenario could possibly have taken place, given the precursor concentrations and reaction conditions.

The reaction medium at the beginning was made up of small (of about ≤ 4 nm diameter) MnCys nanoparticles, unreacted Mn^{2+} ions, and Cys ligand (both of low concentrations), and added Zn^{2+} and acetate ions. Complexation reaction of Zn^{2+} ions with the nanoparticles, through the available reactive sites, which include carboxylate, thiol, and amino groups of the ligands, might have led to the formation of 2D crystalline films. The films would be the result of periodic arrangements of nanoparticles connected by a multitude of chemical bonds between them as mentioned above. The 2D films would have produced angularly twisted moiré superlattices. Probably, the limited, and uncertain accessibility of the reactive sites directed the rotational stacking between the films. At the beginning of the reaction, in the presence of sufficient Zn^{2+} ion concentration, the generation of purely hexagonal 2D films at the surface of MnCys nanoparticles by complexation reaction with Zn^{2+} ion could be a thermodynamically favored process. As soon as the 2D sheets were formed, unavailability of reaction sites to form pure hexagonal stacking triggered a kinetically favored process that would involve bonding between the exposed reactive sites of the films and metal ions (preferably Zn^{2+} ions due to their higher concentrations at the interfaces). The observations of a wide range of angular stacking between the crystalline films would also support the kinetically favored process. The thickness of the moiré films would grow with new stacking with singular crystalline 2D films or already

formed moiré films. TEM images acquired at different times of the reaction revealed a wide range of moiré periods, as well as angles of rotation (Figure 2A-F).

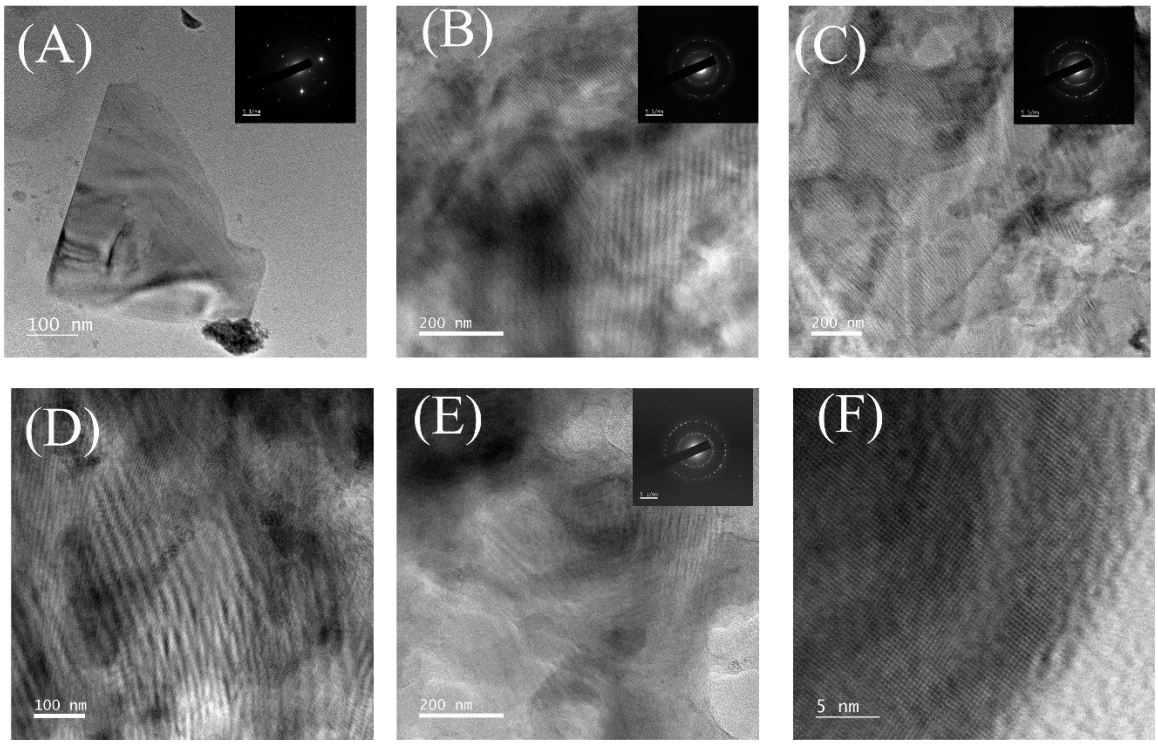

Figure 2. TEM images recorded after (A-B) 3 h, (C-D) 24 h, (E) 72 h of addition of Zn^{2+} to the dispersion of nanoparticles. The figures in the inset represent SAED patterns recorded from the respective area. (F) HRTEM image recorded at the edge of the sheet as is represented in Figure 2A.

The metal complex constituent of the nanoparticle is known to exhibit the Cotton Effect at a wavelength of 318 nm in the circular dichroism spectrum.[12] The nanoparticles however were devoid of any significant circular dichroism peak (Figure 3A-B, spectrum c). As the morphology of the moiré solid involved rotational distortion between the layers, the product 2D films were expected to have been asymmetric. Structural chirality originating from achiral molecules in metamaterials,[38] and bilayer graphene[39] have been reported. The current experiments were carried out with both L-cysteine and D-cysteine. The inorganic complex with L-cysteine exhibited the signature negative cotton effect peak of the complex at 316 nm, whereas the complex with D-cysteine exhibited a positive Cotton effect peak at 319 nm (Figure 3A-B, spectrum a). Two other Cotton effect peaks at 586 nm, and 413 nm for the L-cysteine complex; and 537 nm, and 395 nm for the D-cysteine complex were also observed. The phase

profile for circular dichroism peaks of the metal complexes corresponding to L-cysteine, and D-cysteine were opposite to each other. Interestingly, both of the circular dichroism spectra corresponding to the dispersion containing moiré structure with L-cysteine, and D-cysteine exhibited three distinguished CD peaks at nearly the same wavelengths (Figure 3A-B, spectrum b), and shared the same phase profile. The species involving L-cysteine showed CD peaks at wavelengths of 482 nm, 513 nm, and 643 nm, whereas the D analog exhibited CD signals at wavelengths of 480 nm, 524 nm, and 648 nm respectively.

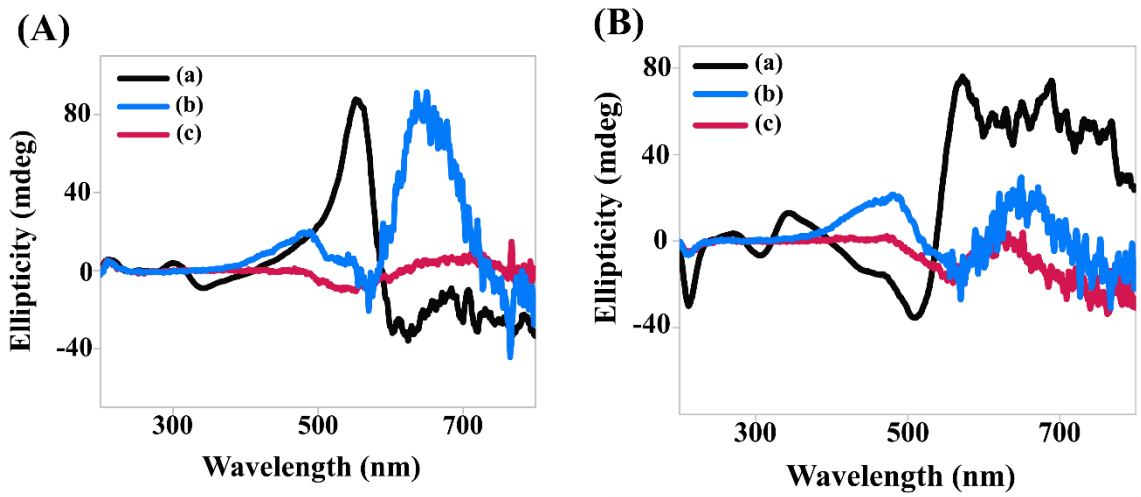

Figure 3. Circular dichroism spectra of (a) the pristine metal complex, (b) the moiré structure, (c) precursor nanoparticles for moiré structure made of the metal complex involving (A) L-cysteine, (B) D-cysteine, respectively.

The chirality of the system was found to be independent of the chiral identity of the constituent optically active ligand, which supported the rotational distortion between the 2D films in the moiré structure.

The unpaired valence electrons of Mn^{2+} ions provided us with an easy opportunity of pursuing the effects of interfacial bonding of the twisted crystals through ESR. The crystalline 2D films can be thought to consist of two different kinds of Mn^{2+} ions. One is the Mn^{2+} (Type I) ions embedded in the cores of the uniform nanoparticles constituting the films. The other kind (Type II) represented those present on the surface of the nanoparticles forming the films. The diamagnetic Zn^{2+} ions would of course bind with the ligands on the surfaces leading to the film formation. When these films would stack angularly against each other, the Mn^{2+} and Zn^{2+} ions forming the films and being present in the vicinity, would come under the influence of the new field due to the interfacial bonding.

In order to know about the local chemical environment of the Mn^{2+} ions present in the system, ESR spectra of the precursor-nanoparticle-dispersion, and the reaction medium dispersion containing moiré-solids were recorded with same experimental parameters (Figure 4A).

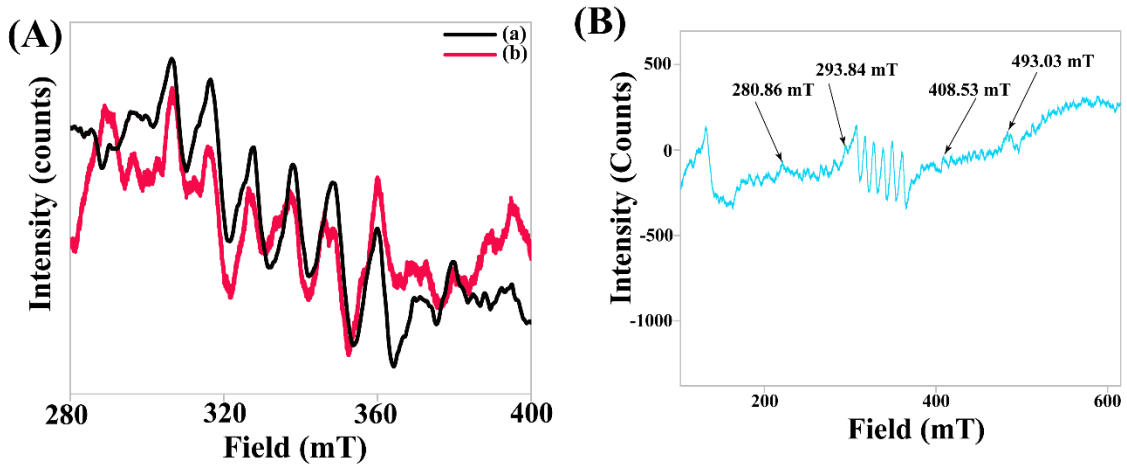

Figure 4. (A) ESR spectra of (a) dispersion containing uniform-sized nanoparticles, and (b) dispersion containing moiré solids using the same experimental parameters. **(B)** ESR spectrum of a dispersion containing moiré solid obtained by evaporating the solvents from different reaction mixtures and then collecting them as a solid following by redispersion.

As is evident from the image (4A spectrum a) the nanoparticles showed distinctive signature hyperfine splitting of Mn^{2+} ion owing to the central electronic transition (m_s =-1/2 to +1/2, $\Delta m_s = \pm 1$, $\Delta m_I = 0$). The center of the signal appeared at a g-value of 2.05116. It is important to be noted here that the reaction-mediated formation of nanoparticles from the precursor metal complex had been discussed in the aspect of ESR spectroscopy in our previous work,[12] where the distinctive signature Mn^{2+} hyperfine pattern disappeared upon the formation of nanoparticles. In order to compare the results, all the experimental parameters were kept unaltered. Here in this case, for recording the ESR spectrum of the uniformly distributed nanoparticles, the parameters were further optimized until the spectrum exhibited signature Mn^{2+} hyperfine splitting, and for current experiments, the parameters were kept unchanged while comparing two or more species (Modulation width 1.2 mT, and amplitude 500 for spectra represented in Figure 4A). The six hyperfine splitting lines inside the central electronic transition ($\Delta m_s = \pm 1$) represent the spin-allowed transitions ($\Delta m_I = 0$).

Importantly, the ESR spectrum of the dispersion containing moiré solids (Figure 4A, spectrum b) was found to exhibit additional small peaks in between the stronger hyperfine

peaks of Mn^{2+}. The g-value was found to be 2.11457, significantly shifted from that of the precursor nanoparticles. As the Mn^{2+} ions in both the complex and the nanoparticle form exhibited g-values close to that of free electrons, here this shift could be a reflection of a substantially different electronic environment possibly introduced to the system by moiré solid. The g-tensor in interlayer exciton has been reported to be affected by twist-angle previously.[40,41] These additional peaks appearing in the span of central electronic transition can be explained by the relaxation of the nuclear spin selection rule from $\Delta m_I = 0$, to $\Delta m_I = \pm 1$.[42–44] Hence, in the case of the ESR spectrum of the moiré solids, the spectrum (Figure 4A, spectrum b) consisted of trivial hyperfine peaks and additional small peaks in between with a shifted g-value. The additional splitting might have been resulted by the presence of type II Mn^{2+} ions residing at the surface of nanoparticles as constituents of the sheets forming the moiré pattern, whereas the nuclear-spin-allowed hyperfine peaks could be resulted by both type-I, and type II Mn^{2+} ions.

Interestingly, four other peaks, occurring at both higher and lower magnetic fields as compared to the central transition, were observed at the magnetic fields of 280.86 mT, 293.84 mT, 408.53 mT, and 493.03 mT. These could be identified as non-central electronic transitions. These non-central electronic transitions might have been resulted by the prevailing additional magnetic field at the interface of the 2D moiré films, which resulted in the alteration of zero-field splitting (ZFS) term (Figure 4A). Local chemical environments, such as alteration of crystal field by ligands, distortion in the geometry of the complex, extent of covalency, and lattice-dimensionality have been known to perturb the ZFS term.[45] Here, the origin of moiré solid by the systematic orientation of nanoparticles, and sheets comprised of the metal complex can also contribute to the crystal field acting on the metal ion, which in turn can lead to the perturbation of the ZFS term. The shifted g-term mentioned earlier can be a mere consequence of the local field introduced in the moiré solid.[46] Hence, the appearance of outer transition peaks in the X-band ESR spectrum upon the formation of moiré solid can be perceived as a consequence of perturbation on the ZFS term. Therefore, in case of metal complex, formation of moiré solid and as a consequence the interfacial field can be considered as a factor that directly influenced the ZFS parameter observed in the extraordinary ESR spectrum reported here.

Conclusion

In summary, the moiré pattern in 2D films was found to be generated by reaction-mediated assembly of MnCys nanoparticles, and Zn^{2+} ion in ambient reaction conditions. The rotationally distorted stacking of 2D crystalline films in the moiré structure was evident by the emergence of ligand-independent chirality of the system, and variation in the chemical environment upon formation of the moiré pattern was successfully probed by ESR spectroscopy. Moiré pattern generated by rotationally stacked 2D films exhibited circular dichroism peaks irrespective of the chiral identity of the ligand. Owing to the generation of the moiré pattern, the hyperfine splitting of Mn^{2+} ion was further split as a result of the relaxation of nuclear spin forbidden transition in ESR spectroscopy. Four non-central electronic transitions upon formation of moiré pattern were observed in X-band ESR spectroscopy implying alteration in zero field splitting term of Mn^{2+} ion. The present discovery enlightens the significance of moiré materials made of inorganic complex nanoparticles with the fusion of the diverse structural, physical, and chemical aspects of constituent metal ions, and ligands.

Author Information

Corresponding Author

Arun Chattopadhyay, Department of Chemistry and Centre for Nanotechnology, Indian Institute of Technology Guwahati, 781039, Assam, India. Orcid ID:0000-0001-5095-6463, Email ID: arun@iitg.ac.in

Author

Archismita Hajra, Centre for Nanotechnology, Indian Institute of Technology Guwahati, 781039, Assam, India. Orcid ID: 0000-0002-1058-8288, Email ID: archismi@iitg.ac.in

Conflicts of Interest

The authors declare no conflicts of interest.

Acknowledgments

This work was supported by the Ministry of Electronics and Information Technology, Government of India (MEITY grant no. 5(1)/2022- NANO). A.C. thanks the Science and Engineering Research Board of the Department of Science and Technology, Government of

India, for a J. C. Bose Fellowship (JCB/2019/000039). Assistance from the Central Instruments Facility (CIF), Centre for Nanotechnology, IIT Guwahati is acknowledged.

References.

[1] J. Chatsirisupachai, P. Nalaoh, C. Kaiyasuan, P. Chasing, T. Sudyoadsuk, V. Promarak, *Mater Chem Front* **2021**, *5*, 2361–2372.

[2] Z. Aliakbar Tehrani, K. S. Kim, *Int J Quantum Chem* **2016**, *116*, 622–633.

[3] C. Kulkarni, K. K. Bejagam, S. P. Senanayak, K. S. Narayan, S. Balasubramanian, S. J. George, *J Am Chem Soc* **2015**, *137*, 3924–3932.

[4] S. Rösel, H. Quanz, C. Logemann, J. Becker, E. Mossou, L. Cañadillas-Delgado, E. Caldeweyher, S. Grimme, P. R. Schreiner, *J Am Chem Soc* **2017**, *139*, 7428–7431.

[5] S. Lv, Y. Wu, K. Cai, H. He, Y. Li, M. Lan, X. Chen, J. Cheng, L. Yin, *J Am Chem Soc* **2018**, *140*, 1235–1238.

[6] J. Hermann, R. A. DiStasio, A. Tkatchenko, *Chem Rev* **2017**, *117*, 4714–4758.

[7] M. H. Y. Chan, V. W. W. Yam, *J Am Chem Soc* **2022**, *144*, 22805–22825.

[8] J. R. Galán-Mascarós, K. R. Dunbar, *Angewandte Chemie - International Edition* **2003**, *42*, 2289–2293.

[9] J. S. Miller, *Angewandte Chemie - International Edition* **2003**, *42*, 27–29.

[10] M. Quesada, V. A. De La Peña-O'Shea, G. Aromí, S. Geremia, C. Massera, O. Roubeau, P. Gamez, J. Reedijk, *Advanced Materials* **2007**, *19*, 1397–1402.

[11] Y. Gong, L. Fu, Y. Che, H. Ji, Y. Zhang, L. Zang, J. Zhao, Y. Che, *J Am Chem Soc* **2023**, DOI 10.1021/jacs.3c01517.

[12] A. Hajra, A. Chattopadhyay, *Langmuir* **2023**, *39*, 8668–8679.

[13] S. Basu, A. Hajra, A. Chattopadhyay, *Nanoscale Adv* **2021**, *3*, 3298–3305.

[14] K. S. Novoselov, A. K. Geim, S. V Morozov, D. Jiang, Y. Zhang, S. V Dubonos, I. V Grigorieva, A. A. Firsov, *Electric Field Effect in Atomically Thin Carbon Films*, Kluwer, **2000**.

[15] D. Geng, H. Y. Yang, *Advanced Materials* **2018**, *30*, DOI 10.1002/adma.201800865.

[16] Y. C. Lin, R. Torsi, R. Younas, C. L. Hinkle, A. F. Rigosi, H. M. Hill, K. Zhang, S. Huang, C. E. Shuck, C. Chen, Y. H. Lin, D. Maldonado-Lopez, J. L. Mendoza-Cortes, J. Ferrier, S. Kar, N. Nayir, S. Rajabpour, A. C. T. van Duin, X. Liu, D. Jariwala, J. Jiang, J. Shi, W. Mortelmans, R. Jaramillo, J. M. J. Lopes, R. Engel-Herbert, A. Trofe, T. Ignatova, S. H. Lee, Z. Mao, L. Damian, Y. Wang, M. A. Steves, K. L. Knappenberger, Z. Wang, S. Law, G. Bepete, D. Zhou, J. X. Lin, M. S. Scheurer, J. Li, P. Wang, G. Yu, S. Wu, D. Akinwande, J. M. Redwing, M. Terrones, J. A. Robinson, *ACS Nano* **2022**, DOI 10.1021/acsnano.2c12759.

[17] J. M. Little, J. Sun, A. Kamali, A. Chen, A. C. Leff, Y. Li, L. K. Borden, T. U. Dissanayake, D. Essumang, B. O. Oseleononmen, D. Liu, T. J. Woehl, P. Y. Chen, *Adv Funct Mater* **2023**, DOI 10.1002/adfm.202215222.

[18] M. Paul, S. Basu, A. Chattopadhyay, *Langmuir* **2020**, *36*, 754–759.

[19] S. Basu, A. Chattopadhyay, *Langmuir* **2019**, *35*, 5264–5270.

[20] P. Das, A. Chattopadhyay, *Journal of Physical Chemistry C* **2022**, *126*, 997–1005.

[21] P. Hu, H. Yang, S. Chen, Y. Xue, Q. Zhu, M. Tang, H. Wang, L. M. Liu, P. Gao, X. Duan, L. Guo, *J Am Chem Soc* **2023**, *145*, 717–724.

[22] Y. Liu, C. Zeng, J. Yu, J. Zhong, B. Li, Z. Zhang, Z. Liu, Z. M. Wang, A. Pan, X. Duan, *Chem Soc Rev* **2021**, *50*, 6401–6422.

[23] M. R. Rosenberger, H. J. Chuang, M. Phillips, V. P. Oleshko, K. M. McCreary, S. V. Sivaram, C. S. Hellberg, B. T. Jonker, *ACS Nano* **2020**, *14*, 4550–4558.

[24] G. Kalita, K. Wakita, M. Umeno, *Jpn J Appl Phys* **2011**, *50*, DOI 10.1143/JJAP.50.070106.

[25] Y. Xiao, J. Liu, L. Fu, *Matter* **2020**, *3*, 1142–1161.

[26] R. Bistritzer, A. H. MacDonald, *Proc Natl Acad Sci U S A* **2011**, *108*, 12233–12237.

[27] E. Y. Andrei, D. K. Efetov, P. Jarillo-Herrero, A. H. MacDonald, K. F. Mak, T. Senthil, E. Tutuc, A. Yazdani, A. F. Young, *Nat Rev Mater* **2021**, *6*, 201–206.

[28] S. Kezilebieke, V. Vaňo, M. N. Huda, M. Aapro, S. C. Ganguli, P. Liljeroth, J. L. Lado, *Nano Lett* **2022**, *22*, 328–333.

[29] T. S. Huang, Y. Z. Chou, C. L. Baldwin, F. Wu, M. Hafezi, *Phys Rev B* **2023**, *107*, DOI 10.1103/PhysRevB.107.195151.

[30] J. Liu, X. Dai, *Nature Reviews Physics* **2021**, *3*, 367–382.

[31] G. Chen, A. L. Sharpe, E. J. Fox, Y. H. Zhang, S. Wang, L. Jiang, B. Lyu, H. Li, K. Watanabe, T. Taniguchi, Z. Shi, T. Senthil, D. Goldhaber-Gordon, Y. Zhang, F. Wang, *Nature* **2020**, *579*, 56–61.

[32] C. R. Dean, L. Wang, P. Maher, C. Forsythe, F. Ghahari, Y. Gao, J. Katoch, M. Ishigami, P. Moon, M. Koshino, T. Taniguchi, K. Watanabe, K. L. Shepard, J. Hone, P. Kim, *Nature* **2013**, *497*, 598–602.

[33] M. Zhang, X. Zhao, K. Watanabe, T. Taniguchi, Z. Zhu, F. Wu, Y. Li, Y. Xu, *Phys Rev X* **2022**, *12*, DOI 10.1103/PhysRevX.12.041015.

[34] A. R.-P. Montblanch, M. Barbone, I. Aharonovich, M. Atatüre, A. C. Ferrari, *Nat Nanotechnol* **2023**, *18*, 555–571.

[35] M. Dressel, S. Tomić, **2020**, DOI 10.1080/00018732.2020.1837833.

[36] X. Wang, Q. Zhang, *SmartMat* **2023**, DOI 10.1002/smm2.1196.

[37] A. Hajra, A. Chattopadhyay, *Langmuir* **2023**, *39*, 8668–8679.

[38] Z. Wu, Y. Liu, E. H. Hill, Y. Zheng, *Nanoscale* **2018**, *10*, 18096–18112.

[39] J. Chi, H. Liu, Z. Wang, N. Huang, *Opt Express* **2020**, *28*, 4529.

[40] K. L. Seyler, P. Rivera, H. Yu, N. P. Wilson, E. L. Ray, D. G. Mandrus, J. Yan, W. Yao, X. Xu, *Nature* **2019**, *567*, 66–70.

[41] Y. G. Gobato, C. S. De Brito, A. Chaves, M. A. Prosnikov, T. Woźniak, S. Guo, I. D. Barcelos, M. V. Milošević, F. Withers, P. C. M. Christianen, *Nano Lett* **2022**, *22*, 8641–8646.

[42] E. Garribba, G. Micera, *Magnetic Resonance in Chemistry* **2006**, *44*, 11–19.

[43] B. Bleaney, R. S. Rubins, *Explanation of s o m e 'Forbidden' Transitions in Paramagnetic Resonance. .. .. . (2)*, **n.d.**

[44] T. A. Stich, S. Lahiri, G. Yeagle, M. Dicus, M. Brynda, A. Gunn, C. Aznar, V. J. DeRose, R. D. Britt, *Appl Magn Reson* **2007**, *31*, 321–341.

[45] D. A. Cleary, A. H. Francis, E. Lifshitz, *ANALYSIS OF THE ESR SPECTRUM OF MANGANESE (II) IN THE LAYERED COMPOUND Cd,P,Sq*, **1986**.

[46] C. Duboc, *Chem Soc Rev* **2016**, *45*, 5834–5847.